Rev. LatinAm. Metal. Mat.

Artículo Regular

www.rlmm.org

SYNTHESIS AND CHARACTERIZATION OF Mg-In ALLOYS (17.47% AT. AND 38.84% AT.) PREPARED BY MECHANICAL ALLOYING

Ney J. Luiggi A., Miguel Rondón, María Valera*

Grupo de Física de Metales. Dpto. de Física. Escuela de Ciencias. Núcleo de Sucre. Universidad de Oriente. Cumaná. Venezuela.

*e-mail: nluiggi51@gmail.com

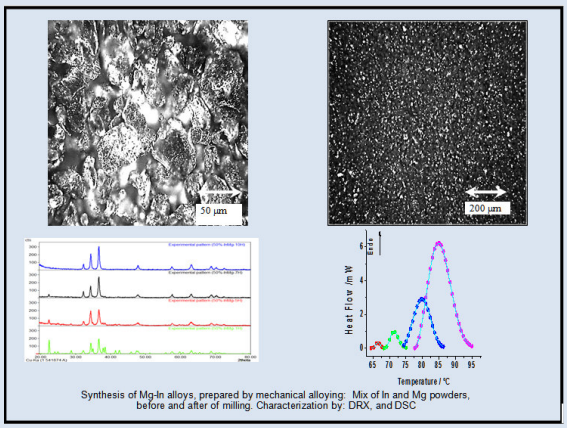

Synthesis of Mg-In alloys, prepared by mechanical alloying: Mix of In and Mg powders, before and after of milling. Characterization by: DRX, and DSC

ABSTRACT

We synthesized two Mg-In alloys, namely, Mg 50% In (17.47% at. In) and Mg 75% In (38.84% at. In) by subjecting high purity Mg and In powders to mechanical alloying. The synthesis was followed in each case by X-ray diffraction (XRD), which allowed for the identification of a series of Mg-In metastable phases that occurred during the alloying process. The invariability of the diffraction patterns made it possible for the grinding time to be set at 10 hours, phases $In_{0.144}$ $Mg_{1.856}$ and $In_{0.212}$ Mg $_{1.788}$ and phases InMg and $InMg_3$ having the greatest presence in the Mg 17.47% at. In and Mg 38.84% at. In alloys, respectively. Samples thermally annealed at 300 and 400 ºC were studied by differential scanning calorimetry (DSC) and electrical resistivity (Δρ). DSC measurements showed a series of endothermal phases according to what is established in the phase diagram of the Mg-In system. A kinetic analysis of the first reactions in both alloys after annealing at 300 ºC evinced that they occurred by indium diffusion in the Mg matrix. When the annealing was at 400 ºC, however, above the solubility limit of both β1 in the case of Mg 17.47% at. In; and β2 in that of Mg 38.84 % at In, reactions revealed low activation energy, mainly due in the first case to the migration of In atoms in the Mg solid solution, and to the order-disorder transition effects in the second. This behavior was ratified by Δρ measurements.

Keywords: *Mg-In alloy, DSC, Electrical Resistivity, DRX, Kinetic analysi*

SÍNTESIS Y CARACTERIZACIÓN DE ALEACIONES MG-IN (17.47 % AT. Y 38.84 % AT.) PREPARADAS POR ALEACIÓN MECÁNICA.

RESUMEN

Mediante molienda mecánica y utilizando polvos de Mg y de In de alta pureza sintetizamos dos aleaciones de Mg-In: Mg 50% In (17.47%at. In) y Mg 75% In (38.84% at. In). En cada caso, la evolución del proceso de síntesis fue seguida por Difracción de Rayos X (DRX*),* lo cual permitió la identificación de una serie de fases metaestables Mg-In que ocurren durante el aleado. La invariabilidad de los patrones de difracción permitió fijar en 10 horas el tiempo de molienda, siendo las fases In $_{0.144}$ Mg $_{1.856}$ e In $_{0.212}$ Mg $_{1.788}$ y las fases InMg e $InMg_3$ las de mayor presencia en la aleación Mg 17.47 % at In y en la aleación Mg 38.84% at In respectivamente. Las muestras compactadas y tratadas térmicamente mediante recocidos a 300 y 400ºC se estudiaron por calorimetría diferencial de barrido (DSC) y por resistividad eléctrica (Δρ). Las medidas de DSC evidencian una serie de reacciones endotérmicas acordes con lo establecido en el diagrama de fases del sistema Mg-In. Un análisis cinético sobre las reacciones correspondientes a la fase β1 y β2 después de un recocido a 300 ºC evidencia que éstas ocurren por difusión del In en la matriz de Mg. Sin embargo, cuando el recocido es a 400 ºC, por encima del límite de solubilidad de la fase β1 en la aleación Mg 17.47% at In y β2 para la aleación Mg 38.84% at In, las reacciones presentan una baja energía de activación en el primer caso causado por la migración de átomos de In en la solución sólida de Mg, y en el segundo caso por efectos de la transición orden-desorden presentes. Este comportamiento es ratificado por las medidas de Δρ.

Palabras claves: *Aleación Mg-In, DSC, Resistividad Eléctrica, DRX, Análisis Cinético.*

Recibido: 16-05-2019 ; **Revisado:** 21-10-2019

Aceptado: 18-12-2019 ; **Publicado:** 27-04-2020

DOI: *10.5281/zenodo.7693707*

pISSN: 0255-6952 | eISSN: 2244-7113

Rev. LatinAm. Metal. Mat. 2020; **40** (1): 15-35

1. INTRODUCTION

Mg alloys are, in general, light and resistant, conditions which confer a multiplicity of industrial uses. Some structural details, typical of Mg crystallization in the hexagonal system, are often transferred to its alloys, a premise which both allows the regulation of certain mechanical properties associated with the reduction of the number of slide planes, and affects the formability of said alloys. Some alloying elements, such as indium, help improve this condition, [1, 2]. In Mg-In alloys, the tetragonal structure of indium contributes its softness, fusibility, and malleability; and although it increases its total density, its low electrochemical activity counters the high electropositive activity of magnesium, making it less reactive and promoting the formation of intermetallic MgIn [3]. The constitution of the Mg-In alloy has been the subject of numerous studies [4-10], these works showing certain inconsistencies regarding the number of intermediate phases, solid state transformations, and peritectic reactions, particularly for In atomic concentrations in excess of 20%, [8,9]. The most common, although ambiguous, designations reported in the literature for the phases present in the Mg-In system are: Primary solid solution of In (Phase γ-tetragonal), primary solid solution of Mg (Phase α-hexagonal), intermediate disordered solid solution Mg (Phase β), Mg_3In (Phase β1-ordered-hexagonal-L12), Mg_2In (Phase β2-ordered-hexagonal), Mg_5In_2 (Phase β3-D8g), $Mg_{1.2}$ $In_{2.8}$ (Phase γ '-L12), MgIn (Phase β'-ordered FCC-$L1_0$) [8], MgIn (Phase β"-ordered tetragonal-$L1_0$) [8], and $MgIn_3$ (Ordered phase γ') [11], Mg_2In_5 (Phase β'"-ordered orthorhombic) [12,13].

Unlike the above-referenced works, where the alloys are prepared by fusion, the work at hand involved two mechanically processed Mg alloys containing 17.47% at. and 38.84% at. In. Few references to Mg-In alloys prepared by mechanical alloying are reported in the literature. After evaluating some characteristic parameters of the constitution of several Mg alloys by this synthesis method, Liang *et al.* [14] reported that a high solubility of indium is retained in Mg at room temperature. Diffractograms of one such alloy, Mg 10% at. In, revealed the sole presence of Mg peaks since only the α solid solution of Mg was present at that concentration. For the Mg 17.47% at. In, particularly, the phase diagram of Nayeb *et al*. [8] shown in Figure 1 revealed the presence of an α + β1 phase at low temperatures and a solid α solution between 318 ºC and 495 ºC, the limit of solubility being 318 ºC and the corresponding α + liquidus region, 495 °C; whereas for the Mg 38.84% at. In, the phase diagram showed a β" + β2 phase, a β", the disordered β phase, and the region corresponding to β + liquidus, at 411 ºC. Our objective was to synthesize Mg-In alloys by processing them mechanically; to visualize and monitor the structural changes occurring in the alloys during the alloying process by optical microscopy and XRD; and to characterize them by both electrical resistivity and differential scanning calorimetry (DSC). A kinetic study of the transformations occurring in samples annealed at 300 ºC and 400 ºC, derived from the calorimetric curves, is presented.

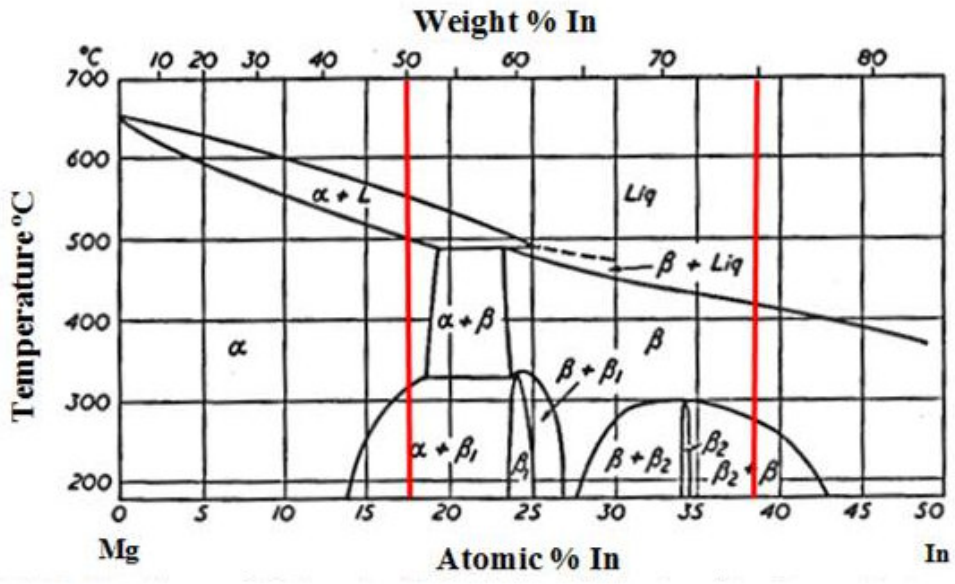

Figure 1. Phase diagram of Mg-In system [8], showing in red the location of the alloys used in the present work.

2. EXPERIMENTAL PART

Elemental Mg and In powders with a purity greater than 99.9%, manufactured by Sigma-Aldrich and RotoMetals, respectively, were used as precursor materials, the particles of the former being smaller than 200 μm and those of the latter, smaller than 1000 μm. The mechanical alloying was carried out in a FRITSCH Pulverisette 7 premium line ball mill with a rotation speed of up to 1110 rpm and a centrifugal acceleration of up to 95 g. It integrates two steel vials sealed under an argon atmosphere. Stainless steel balls were used, the ball-powder mass ratio being 1:10. In our case, to avoid overheating, the total grinding time was programmed in cycles of 1 continuous hour of grinding with 15-minute rest intervals. Power X-diffraction was performed with a Panalytical X-Pert-Pro diffractometer equipped with a PW3040/60 console and a CuKα radiation wavelength of 1.541874 Å. The heat flow of the samples was measured in an extra pure argon environment using a Perkin Elmer DSC 7 calorimeter with a TAC 7/DX DSC thermal analysis controller. Samples with a diameter of 6 mm and a mass ranging between 25 and 30 mg were analyzed in aluminum sample pans. The electrical resistivity measurements were performed with a SIGMATEST 2.069 microprocessor controller in accordance with the eddy currents method. The microstructure of the alloys was studied by setting etched samples in a diluted 5% Nital solution and observing them under an Olympus CK40M optical microscope at very short intervals of time. Electrical resistivity and DSC studies were performed by subjecting compacted and annealed samples to 400 °C and 300 °C for 1 hour and then quenching them in water at 3°C.

3. RESULTS AND DISCUSSION

3.1 Optical microscopy

Once the alloys were synthesized, their homogeneity was checked by light microscopy, which allowed a detailed observation of their microstructure. Figure 2 shows two different stages of the synthesis of Mg 17.47% at. In, one right after the initial mixing of Mg and In powders; and the other after 10 hours of grinding, the homogeneity of the sample annealed at 300 °C being reached after milling. The microstructural details of the powders are also shown after compaction and annealing for 1 hour at 300 °C.

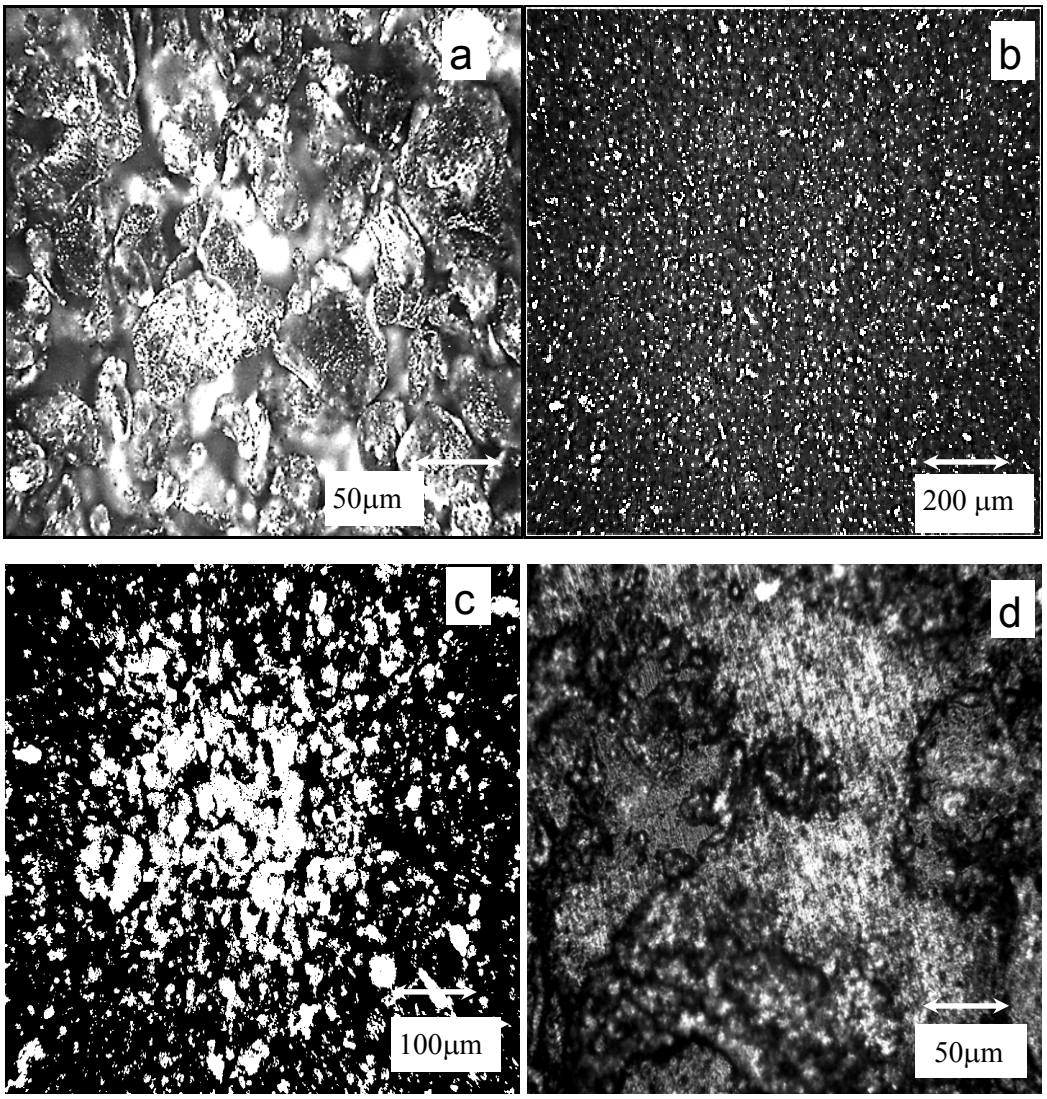

Figure 2. Optical micrographs of the Mg 17.47% at. In alloy. a. Initial mix of Mg and In powders. b. and c. Powders after 10 hours of milling at different magnifications. d. Compacted powders after 10 hours of milling. The white spots correspond to indium particles. Etching was carried out with a Nital solution at different exposure times.

Figure 3 shows two different stages in the synthesis of the Mg 38.84% at. In alloy. Figures 3a and 3b show the distribution of indium (white spots) and magnesium (dark spots) after 10 hours of milling. Figure 3c shows the microstructural details of the powders after compaction and annealing for 1 hour at 300 °C, whereas Figure 3d shows the same alloy with elongated grains as a result of grinding, and the advance of recrystallization by subgrain formation inside the primary grains, after subsequent annealing at 300 ºC.

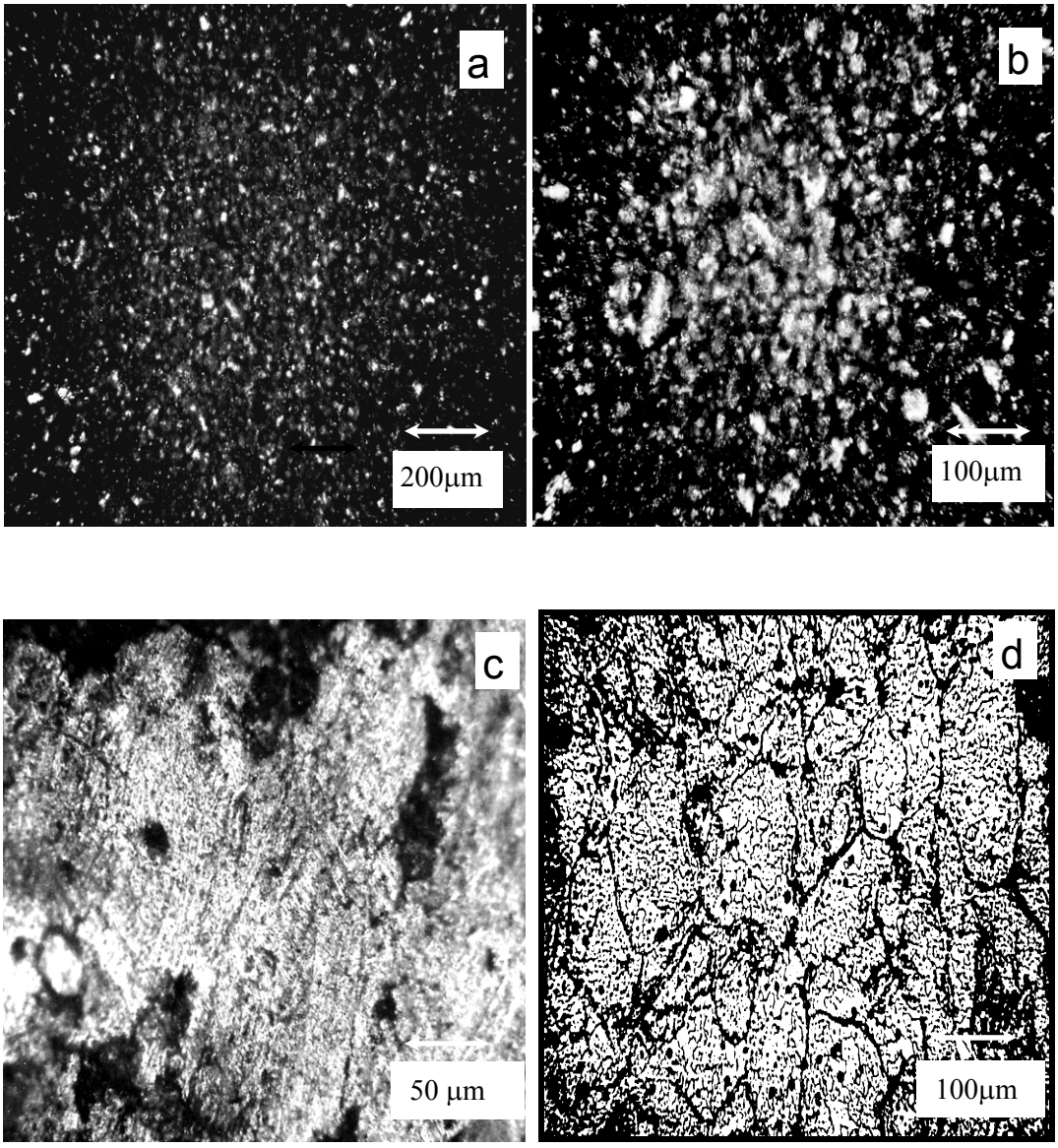

Figure 3. Optical micrographs of the Mg 38.84% at. In alloy. a. and b. After 10 hours of milling at different magnifications. c. Compacted powders after 10 hours of milling. The white spots correspond to indium particles. d. Recrystallization after different stages at 300 ºC. Etching was carried out with a Nital solution at different exposure times.

3.2 X-ray diffraction study

3.2.1 Synthesis of Mg 17.47% at. In

After synthesizing the powders by mechanical alloying, the samples were subjected to X-ray diffraction. Phase identification from powder diffraction data was performed using Match! 3, a Crystal Impact software application, with Kα radiation of Cu of λ = 1.541874 Å. Figure 4 shows the diffractograms obtained using Mg and In powders in equal mass proportions: (Mg 17.47% at. In), for different milling times (1, 5, 7, and 10 hours) with a 2θ angular variation between 20 and 80º. It shows the effect of grinding on the consolidation of the different phases present. At 1 hour of grinding a variety of peaks appeared, some tending to disappear, as in the case of 2θ values <30º, whereas others regulated their FMW and modified their intensity. At 7 hours of milling the alloy seemed to consolidate, presenting at 10 hours only variations in both the intensity of the peaks and their FMW, but not in their position.

Some details of the respective diffractograms, which made it possible to follow the evolution of the phases during milling, are presented below.

The diffractogram corresponding to Mg17.47% at. after 1-hour milling shows the presence of unmixed pure Mg and In phases (Figure 4.a), their respective codes in the COD-Inorganic base being 96-901-3059 (hexagonal space group 194, and lattice parameters a = 3.21470 Å, c = 5.22030 Å) and 96-153-9141 (tetragonal, spatial group 139 with lattice parameters a = 2.7889 Å, c = 4.29300 Å). These patterns, selected from a group of Mg and In diffraction configurations, yielded the highest figures of merit, the main diffraction lines of these phases corresponding to angles 2θ = 36.55, 34.33, and 32.13 for Mg planes (101), (002), and (100); and 2θ = 38.46, 45.98, and 42.06, for In planes (101), (110), and (002). A separation between the positions of their peaks and those of the experimental peaks was detected. The matching process was not completed, an adjustment close to 60% having been achieved with the selected phases, leaving only the indium line corresponding to plane (101) slightly invariable in position (Δ2θ ~ 0.054º). The phases with the greatest presence in this milling stage were $In_{0.212}$ $Mg_{1.788}$, $In_{0.144}$ $Mg_{1.856}$, MgO, Mg_3In, Mg, InMg, In, In_2 MgO_4, and In_2O_3.

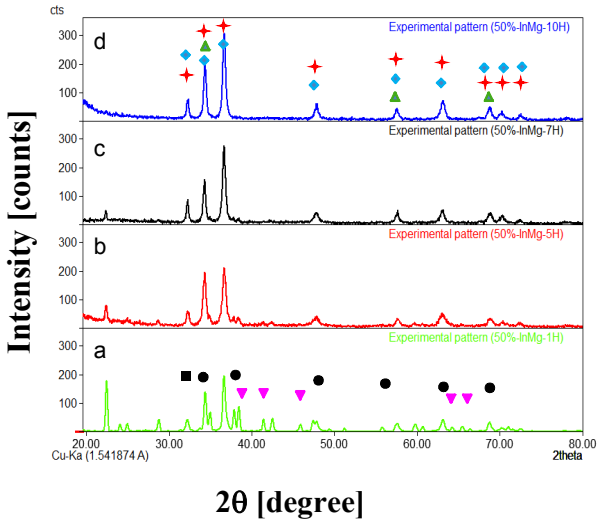

Figure 4. Diffractogram of the Mg 17.47% at. In alloy at different milling times: a: 1 hour; b: 5 hours; c: 7 hours; d: 10 hours. ✦ In 0.144 Mg 1.856 ; ◆ In 0.212 Mg 1.788 ; ▲ InMg3 ; ● Mg ; ▼ In.

The experimental pattern also shows that the three largest peaks were located at 36.65º, 22.45°, and 34.37°, the interplanar distance of the first being 2.4499 Å, adjusted to phases $In_{0.212}$ $Mg_{1.788}$, $In_{0.144}$ $Mg_{1.856}$, and Mg O, Mg; that of the second, 3.9573 Å, not matched; and that of the third, 2.6068 Å, adjusted to phases $In_{0.212}$ $Mg_{1.788}$, $In_{0.144}$ $Mg_{1.856}$, and In Mg_3, In Mg. The crystallite average sizes associated with the three above-referenced most important peaks, as estimated from the Scherrer formula [15], were 112.23 nm, 73.82 nm, and 52.03 nm, respectively. This formula does not consider the lattice strain present in the powder, its construct constituting a simple analysis which overestimates the real size of the crystallites [16, 17]. Considering that the synthesis of the alloy was incomplete, the processes of indexing and refining parameters at this stage did not yield reliable results.

The phases with the greatest presence after 5 hours of milling (Figure 4.b) were: $In_{0.144}$ $Mg_{1.856}$, Mg, MgO, In, In Mg_3, MgO (2), and InMg, comprising a peak area of 60%, identified above, 80% of which, in turn, made up of In $_{0.144}$ $Mg_{1.856}$ and Mg phases. The crystallite sizes deduced from the three most important peaks were 113.1 nm for the main peak, located at 2θ = 36.69° matched to the $In_{0.144}$ $Mg_{1.856}$ phase; 31.70 nm for the second peak at angular position 2θ = 34.33º matched to phases $In_{0.144}$ $Mg_{1.856}$, Mg, In Mg_3, and In Mg; and 57.9 nm for the peak located at 22.42º, not matched to any of the phases indicated. The presence of phases different

from those obtained in the previous diffractogram indicated an ongoing developing process.

For 7 hours of milling (Figure 4.c), the majority of phases corresponded to $In_{0.144}$ $Mg_{1.856}$, $In_{0.212}$ $Mg_{1.788}$, $InMg_3$, MgO, In, Mg, and $In_{1.3}$ $Mg_{0.7}$, representing 75% of identified peaks, phases $In_{0.144}$ $Mg_{1.856}$ and $In_{0.212}$ $Mg_{1.788}$ covering 90% of them. At this stage the crystallite sizes deduced from the three most important peaks were 32.36 nm for the main peak located at 2θ = 36.79º matched to phases $In_{0.144}$ $Mg_{1.856}$, $In_{0.212}$ $Mg_{1.788}$, MgO, In, and $In_{1.3}$ $Mg_{0.7}$; 39.21 nm for that at angular position 2θ = 34.43º matched to phases $In_{0.144}$ $M_{1.856}$, $In_{0.212}$ $Mg_{1.788}$, and In Mg_3; and 74.52 nm for the one located at 32.39º, matched to phases $In_{0.144}$ $Mg_{1.856}$, $In_{0.212}Mg_{1.788}$, and $InMg_3$. DICVOL indexing reproduced the same rhombohedral phase obtained after 5 hours of grinding.

Table 1. Size of crystallites for different peaks estimated from the Scherrer formula [15] for Mg 17.47% at. In obtained after 10 hours of milling. The lattice strain present in the podwer is not considered [16, 17].

2θ / degree	d / Å	I/I0	Phases	*Crystallite size / nm*
36.734	2.447	1000.0	$In_{0.144}$ $Mg_{1.856}$, $In_{0.212}$ $Mg_{1.788}$, Mg O, In	34.73
34.421	2.606	658.5	$In_{0.144}$ $Mg_{1.856}$, $In_{0.212}$ $Mg_{1.788}$, $InMg_3$, In Mg	37.89
32.334	2.769	225.2	$In_{0.144}$ $Mg_{1.856}$, $In_{0.212}$ $Mg_{1.788}$	81.47
63.196	1.471	196.4	$In_{0.144}$ $Mg_{1.856}$, $In_{0.212}$ $Mg_{1.788}$	-
47.936	1.898	173.7	$In_{0.144}$ $Mg_{1.856}$, $In_{0.212}$ $Mg_{1.788}$, In	25.36
68.879	1.363	139.1	$In_{0.144}$ $Mg_{1.856}$, $In_{0.212}$ $Mg_{1.788}$, $InMg_3$, In, In Mg	30.42

The details of the diffractogram obtained after 10 hours of grinding are shown in Figure 4.d. That figure shows nine diffraction peaks suitably matched to pattern In0.144 Mg1.856. The Mg appearing as a pure phase for lower milling times disappeared as such and was integrated to dominant phases In0.144 Mg1.856 and In0.212Mg1.788, these in turn representing 93.15% of the total of peaks matched. The size of crystallites evaluated by the Scherrer formula for the steeper peaks is shown in Table 1, with an average value of 41.974 nm.

Indexing by using DICVOL and considering all the important peaks provided two crystalline structures with a high figure-of-merit. The first one crystallized in the hexagonal system, with lattice parameters a = 3.19938 Å c = 5.20922 Å and equal volume 46.18Å^3, with an average discrepancy of 1.142x10^{-4} and an angular error of 0.01047º. Table 2 shows the crystallographic details of this phase (Miller indices and interplanar distances, expanded directly from the experimental patterns and calculations).

The difference in lattice parameters of the phase indexed with phase $In_{0.144}$ $Mg_{1.856}$ was $\Delta a = -9.2 \times 10^{-4}$ Å and $\Delta c = -3.58 \times 10^{-3}$ Å; while the difference with phase $In_{0.212}$ $Mg_{1.788}$ was $\Delta a = 3.19 \times 10^{-3}$ Å and $\Delta c = -5.38 \times 10^{-3}$ Å. This phase corresponded, within its experimental margin, with phases $In_{0.144}$ $Mg_{1.856}$ and $In_{0.212}$ $Mg_{1.788}$.

The second high figure-of-merit structure calculated by DICVOL was orthorhombic, with lattice parameters a = 5.20930 Å, b = 3.19952 Å, c = 2.777039 Å and volume = 46.17 Å^3, with an average discrepancy of 1.032x10^{-4} and an angular error of 0.009634º. The crystallographic details of this phase are shown in Table 3. It is worth noticing that this

structure failed to match the experimental peak corresponding to plane (1 2 1), a failure which would condition the possibility of considering it with certainty as a new phase for the alloy despite the remarkable coincidence of two of its parameters with those of most phases previously indexed.

Table 2. Indexing of the hexagonal highest figure-of-merit phase for the Mg 17.47% at. In alloy after 10 hours of milling.

h k l	d_{OBS}/ Å	d_{CAL}/ Å	$2\theta_{OBS}$/ degree	$2\theta_{CAL}$/ degree
1 0 0	2.769	2.771	32.332	32.311
0 0 2	2.606	2.605	34.418	34.434
1 0 1	2.447	2.446	36.732	36.740
1 0 2	1.898	1.898	47.932	47.937
1 1 0	1.599	1.599	57.620	57.623
1 0 3	1.472	1.471	63.190	63.197
1 1 2	1.363	1.363	68.872	68.883
2 0 1	1.339	1.339	70.323	70.315
0 0 4	1.302	1.302	72.611	72.595

Table 3. Indexing of the orthorhombic phase of highest merit for the Mg 17.47% at. In alloy after 10 hours of milling

h k l	d_{OBS}/ Å	d_{CAL}/ Å	$2\theta_{OBS}$ /degree	$2\theta_{CAL}$/ degree
0 0 1	2.769	2.770	32.332	32.315
2 0 0	2.606	2.605	34.418	34.433
1 0 1	2.447	2.446	36.732	36.744
2 0 1	1.898	1.898	47.932	47.940
0 2 0	1.599	1.599	57.620	57.620
3 0 1	1.476	1.471	63.190	63.199
2 2 0	1.363	1.363	68.872	68.880
1 0 2	1.339	1.339	70.323	70.325
1 2 1	1.339	--	70.315	--
4 0 0	1.302	1.302	72.611	72.594

3.2.2 Synthesis of Mg 38.84% at. In alloy

The diffraction procedure for Mg 38.84% at. In was similar to that of the previous case. Diffraction studies were carried out at different milling times, all of them showing a tendency towards consolidation after 10 hours. In the intermediate stages, the peaks of greater intensity were located at 2θ <45º, mainly a result of competition between Mg, In, and MgO phases; and to a lesser degree, of that between In and Mg compounds. Figure 5 shows the diffractograms obtained using Mg and In powders in equal 25-75 mass proportions: (Mg 38.84% at. In), for different milling times (5, 7, and 10 hours) with a 2θ angular variation between 20 and 80º.

Figure 5 shows up to 16 consolidated peaks obtained after 10 hours of milling, predominantly conjoined with the InMg phase (phase β ") (P 4 / mmm, tetragonal, a = 4.5800 Å c = 4.3920 Å), covering 58.2% of the total peak area, the other phases present being In Mg_3 (F m -3m, cubic, a = 4.5130 Å) and $In_{0.144}$ $Mg_{1.856}$ (P 63 / mmc, hexagonal, a = 3.2003 Å c = 5.2128 Å), comprising 15.8 and 6.5%, respectively, for a total of 80.5% of covered area after Reitveld refinement. The average crystal size deduced from the highest intensity peaks is shown in Table 4, commanding an average value of 33.6014 nm.

DICVOL indexing of the strongest peaks provided two high figure-of-merit crystalline structures: The first one, a tetragonal arrangement with lattice parameters a = 4.575295 Å, c = 4.38050 Å, volume = 91.6984 $Å^3$, with an average discrepancy of $1.815x10^{-04}$ and an angular error of 0.01482º. The lattice parameters of this structure differed from those reported for the MgIn phase $\Delta a = -4.705 \times 10^{-3}$ Å and $\Delta c = -1.15 \times 10^{-2}$ Å, thus evincing its reality.

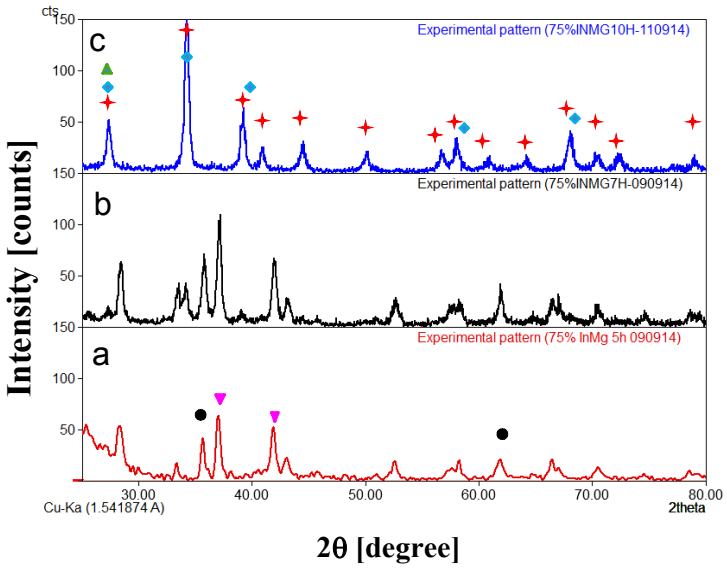

Figure 5. Diffractogram of the Mg 38.84% at. In alloy at different milling times: a: 5 hours; b: 7 hours; c: 10 hours. ✦ In Mg ; ◆ InMg3; ▲ In 0.144 Mg 1.856; ● Mg ; ▼ In.

The second structure crystallized out in the orthorhombic system, with lattice parameters a = 9.14627 Å, b = 4.57728 Å, c = 4.38466 Å, and volume = 183.56 $Å^3$, with an average discrepancy of $1.866x10^{-04}$ and an angular error of 0.01589º. Table 5 shows the crystallographic details of this phase; to wit, Miller indices and interplanar distances taken directly from both the experimental and the calculated patterns.

The parameters of this phase contrasted with those obtained for the matching phases, which after Rietveld refinement [18] reflected the values shown in Table 6. The same table also shows the Miller indices corresponding to both the greater intensity reflection plane of the new phase and the dominant phases of the alloy.

The XRD analysis evinced the coexistence of two phases for the Mg 17.47% at. In alloy, to wit: $In_{0.144}$ $Mg_{1.856}$ and In $_{0.212}$ Mg $_{1.788}$; and the presence of the MgIn phase for the Mg 38.84% at. In, the existence of a second orthorhombic phase being feasible.

Figure 6 shows the diffractograms fitted by using Rietveld refinement for the two alloys under study.

Table 4. Size of crystallites for different peaks obtained from the Scherrer formula [15] for Mg 38.84% at. In alloy. The lattice strain present in the powder is not considered [16,17].

2θ /degrees	*d /Å*	*I/Io*	*Phases*	*Crystallite size /nm*
34.444	2.604	1000.0	In Mg, In Mg_3 In $_{0.144}$ Mg $_{1.856}$	29.10
39.395	2.287	358.9	In Mg, In Mg_3	25.66
27.569	3.236	301.2	In Mg	42.18
68.234	1.375	207.8	In Mg	26.44
44.665	2.029	169.8	In Mg	25.21
41.107	2.196	136.3	In Mg	25.39
58.235	1.584	126.5	In Mg	61.23

Table 5. Indexing the higher figure-of-merit orthorhombic phase for the Mg 38.84% at. In alloy after 10 hours of milling.

h k l	d_{OBS}/ å	d_{CAL}/ å	$2\theta_{OBS}$/ *degrees*	$2\theta_{CAL}$/ *degrees*
0 0 1	4.380	4.385	20.274	20.253
2 1 0	3.236	3.235	27.569	27.572
2 1 1	2.604	2.603	34.444	34.452
0 2 0	2.287	2.289	39.395	39.371
3 1 1	2.196	2.196	41.107	41.101
0 2 1	2.029	2.029	44.665	44.665
2 1 2	1.813	1.815	50.319	50.275
4 2 0	1.618	1.618	56.906	56.927
5 1 1	1.584	1.584	58.235	58.251
4 2 1	1.517	1.518	61.077	61.061
6 1 0	1.446	1.446	64.434	64.423
2 3 1	1.375	1.374	68.234	68.240
2 1 3	1.332	1.332	70.704	70.734
3 3 1	1.303	1.303	72.571	72.562
2 3 2	1.208	1.208	79.291	79.326

Table 6. Comparison of parameters of the new phase and related phases. The reflection planes shown correspond to the peak of greatest intensity in the diffractograms under study.

Phase	*Structure*	2θ	*h k l*	*a*	*b*	*C*
New	Orthorhombic	34.452	2 1 1	9.1463	4.5773	4.3847
InMg	Hexagonal	34.38	1 1 1	4.580	4.5800	5.3920
$InMg_3$	Cubic	34.39	1 1 1	4.5130		
$In_{0.144}Mg_{1.856}$	Hexagonal	34.38	0 0 2	3.1962	3.1962	5.2146

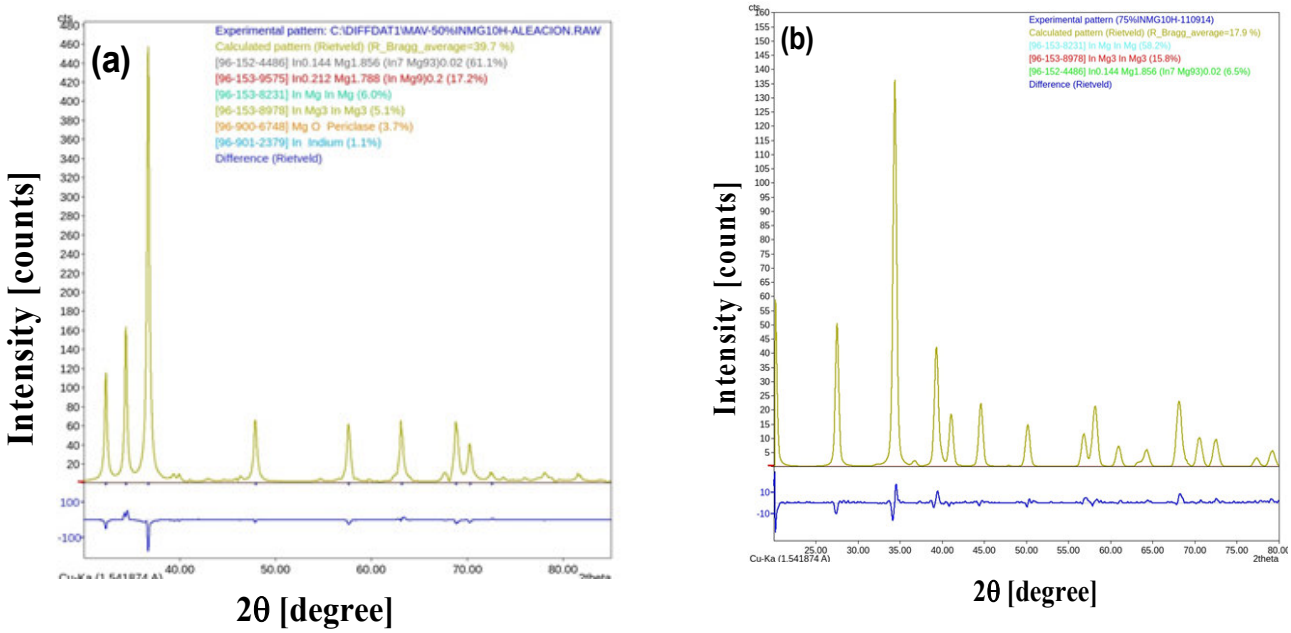

Figure 6. Diffractogram of a) Mg 17.47% at. In alloy and b) Mg 38.84% at. In alloy at 10 hours of milling, showing the Rietveld refinement (—) and the difference between experimental and Rietveld refinement (—).

The indices for each of the phases identified after refinement are:

For Mg 17.47% at. In: In_7 Mg_{93} 0.02(In0.144Mg1.856): 61.1%, In Mg_9 0.2

(In0.212Mg1.788): 17.2%, In Mg (In Mg): 6.0, $InMg_3$ (In Mg_3): 5.13%, Periclase (Mg O): 3.7%, Indium (In): 1.1%.

For Mg 37.8% at. In: In Mg (In Mg): 58.2%, In Mg_3 (In Mg_3): 15.8%, In_7 Mg_{93} 0.02 In0.144 Mg1.856): 6.5%.

3.3 Calorimetric study

3.3.1 Analysis of thermograms

Once synthesized, the alloys were compacted into discoidal pellets with a 6 mm diameter and a mass between 25 mg and 30 mg. To reduce the residual grinding stress and subsequent compaction, the samples were annealed for 1 hour at 400 ºC, which placed them in the domain of phase α (Mg) for the alloy containing 17.47% at. In; and in the domain of the disordered β-phase, for the Mg 38.84% at. In alloy. Similarly, annealing other samples at 300 ºC placed them in the α + β1 region and at the limit of the ordered β'' phase, respectively. The calorimetric study was carried out from 25 ºC to 400 ºC at different heating ϕ rates with the intention of having access to the kinetic parameters of the reactions. The precise temperature range where each structural transformation occurred was determined from the derivation of the measured heat flow with respect to the temperature. Each endothermic or exothermic transformation is represented by a peak or valley on the heat flow curve, mathematically implying a starting point, another point of arrival, two points of inflection, and a maximum (or a minimum in the case of a depression). If the reaction were a peak, its derivative would present a maximum and a minimum respectively associated with the points of inflection of the reaction (or the opposite if it is a valley), the maximum value of the reaction being found at the temperature where the line joining the beginning and end of the derivative intersects that between the maximum and minimum of said curve.

Figure 7 shows the heat flow derivative with respect to the temperature in a Mg 17.47% at. In alloy sample annealed for 1 hour at 300 °C and quenched in chilled water (~ 3°C) for different heating rates. This Figure shows that in this case, only two important endothermic transformations took place, which were displaced as the rate of heating increased. The figure shows an incipient exothermic fluctuation at the beginning of the first transformation. This non-normalized fluctuation was apparently more important for the highest heating rates and could be a consequence of the humidity adsorbed on the sample. Table 7 shows the details obtained for each of the samples studied. The temperature range column indicates the temperature corresponding to the start of the transformation for the curve with the lowest heating rate (5 ºC min^{-1}) and the end temperature of the reaction taken from the curve with the highest one (40 ºC min^{-1}, thus defining the temperatures at both ends of the range where reactions occurred for the different heating rates used.

Considering the Mg-In phase diagram of Nayeb et al. [8], two endothermic transformations can be inferred to have occurred for the Mg17.47 at. In alloy annealed at 300 ºC, the first one corresponding to the dissolution of phase β1; and the second, located just at the solubility limit of the alloy for said concentration, corresponding to the α + β1→α transition. Phase β1 was detected for the same alloy when annealed at 400 ºC, but the temperature range of coexistence for this phase (77 ºC) was much higher than that reported for the sample annealed at a lower temperature. A transformation, not visible in the previous case and only important for the lower heating rates, appeared within a 27 °C temperature range.

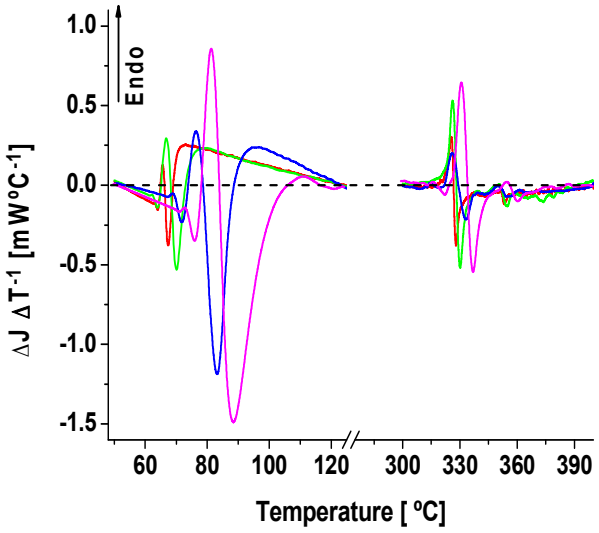

Figure 7. Heat flow derivative with respect to temperature vs. temperature for a Mg 17.47% at. In alloy sample annealed for 1 hour at 300 ºC and measured at different heating rates (ϕ). —: 5 ºC min^{-1}; —: 10 ºC min-1; —:20 ºC min-1; —: 40 ºC min^{-1}

Two endothermic transformations tending to overlap and followed by one of undefined behavior, perhaps due to its proximity to the α + liquidus limit (indicated in the table as endothermic), appeared for the temperatures within the solubility limit range. For the Mg 38.84% at. In annealed at 300 °C, only one endothermic transformation was detected in the region where Nayeb et al. [8] report the presence of β" + β2. No significant thermal response was detected at higher temperatures.

Four endothermic transformations, generally preceded by an incipient exothermic fluctuation, were detected for the same alloy annealed at 400 ºC. The first one, with a temperature range of 59 ºC, was framed within the limits of the biphasic β" + β2 region. The second, between 319 °C and 331 °C and above this biphasic region, corresponded to phase β". The third transformation, between 326 °C and 347 °C, which tended to overlap with the second and coincided with the metastable region represented by Nayeb et al. [8] with dashed lines, was associated with the β" to β order-disorder transition phase. The fourth transformation corresponded to the disordered β phase.

3.3.2.- Kinetic analysis

A brief study of the better-defined structural transformations obtained in this calorimetric study is now presented in order to showcase details of the kinetics of phase formation and the mechanisms promoting it. We selected the first reaction of the four cases depicted in the table, corresponding to the formation of phase β1 in the Mg17.47% at. In and of phase β2 in the Mg38.84% at. In alloys. We followed the methodology used by Luiggi [19] and by Luiggi et al. [20, 21], as depicted below.

1. In order to ascertain whether the heat flow curve as a function of temperature represented a monophasic or a multiphasic reaction, the plots experimentally obtained were individually deconvolved.

2. The activation energy of the process was determined by isoconversion, a calculation expandable from the Kissinger relation if the pair (ϕ, Tmax) is known, which generated a unique activation energy value; or by calculating the transformed fraction as a function of the temperature from the heat flow vs. the temperature curve.

Table 7. Range of coexistence of the different transformations present in the thermograms measured by DSC

Samples	*Anneal Temperature*	*Number of Reactions*	*Temperature Range /ºC*	*Transformation type*
Mg 17.47% at. In	300ºC	2	64.42-95.67 (31.25)	Endothermic
			319.00-346.34 (27.34)	Endothermic
Mg 17.47% at. In	400ºC	5	67.08-144.34 (77.26)	Endothermic
			151.58-178.97 (27.39)	Endothermic
			304.25-323.67 (19.42)	Endothermic
			323.25-335.00 (11.75)	Endothermic
			346.16-385.73 (39.57)	Endothermic
Mg 38.84% at. In	300ºC	1	64.42-95.00 (30.58)	Endothermic
Mg 38.84% at. In	400ºC	4	64.83-123.67 (58.84)	Endothermic
			319.00-331.28 (12.28)	Exothermic
			326.03-347.00 (20.97)	Exothermic
			371.02-398.17 (27.15)	Endothermic

From this curve, the values of the transformed fraction were fixed and the pair (ϕ, T) was obtained for each transformed fraction. The first method is a particular case of the second when T = Tmax. We were thus able to have access to the activation energy variation as a function of the transformed fraction.

3. Once the activation energy was known, we proceeded to evaluate the characteristic parameters of the kinetics by defining a kinetic model, in our case, the truncated Sestak-Berggren model [22,23].

a. Application to the Mg 17.47% at. In alloy

Figures 8.a and 8.b show the heat flow as a function of temperature for the Mg 17.47% at. In alloy, annealed for 1 hour at both 300 °C and 400 °C for different heating rates in the temperature range corresponding to the first reaction. The kinetics resulting from the deconvolution for the sample annealed at 400 °C are also shown.

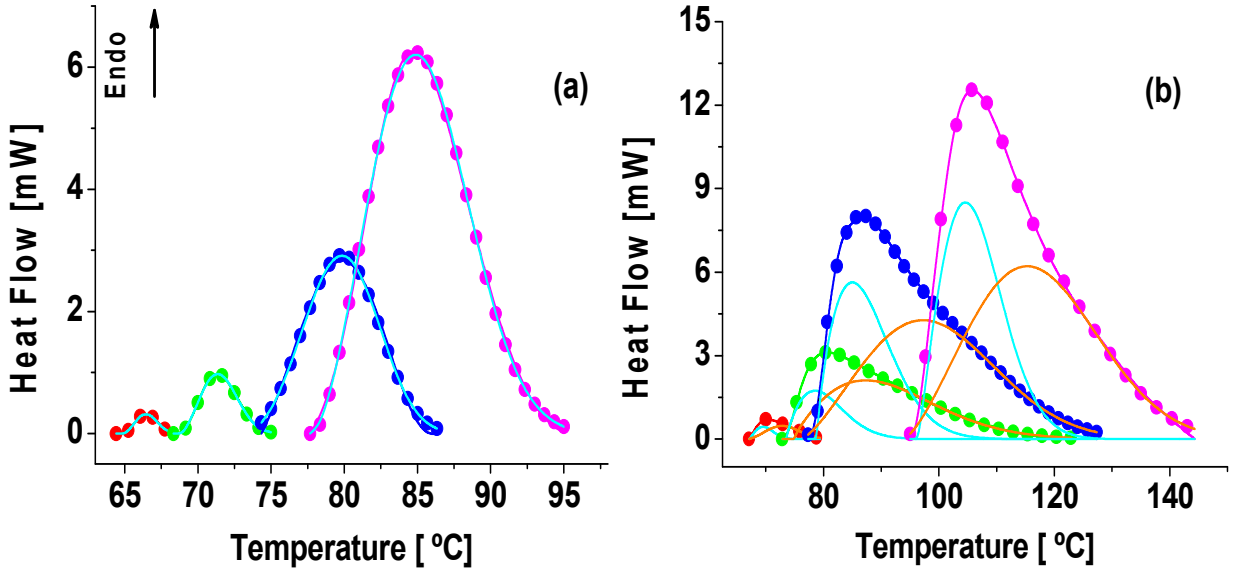

Figure 8. Heat Flow vs. Temperature for an Mg 17.47% at. In alloy using different heat rates. ●5ºC min-1, ●: 10ºC min-1, ●: 20ºC min-1, ●: 40ºC min-1. —: First reaction, —: Second reaction. a) Annealing at 300 ºC. b) Annealing at 400 ºC

Figure 8 shows transformations occurring by diffusion, although a noticeable annealing effect on the heat flow is also shown. Annealing at 400 °C generated for this transformation a temperature range much higher than that shown in samples annealed at 300 °C. The figures are different. The first one represents a single reaction within the deconvolution range applied using Weibull transfer functions with R2 ≥ 0.99. The second depicts at least two reactions, under the same calculation conditions, to reach the same value of R2 when the sample was annealed for 1 hour at 400 ºC. The explanation for this behavior is that the 300 ºC annealing allowed the formation of phase β1, which following quenching, dissolved endothermically as the temperature increased, typified in our results as a single reaction. Annealing the alloy at 400 °C, on the other hand, initially generated the appearance of a solid solution α, with the subsequent precipitation of β1 (previously described as incipient) occurring after quenching, followed by an important endothermic transformation that decomposed into two reactions upon deconvolution via a Weibull transfer function, the first one in agreement with that shown in the previous reaction (β1); and the second, also in the α + β1 region, possibly corresponding to an atomic rearrangement of that phase.

b. Application to the Mg 38.84% at. In alloy

Figures 9.a and 9.b show the heat flow as a function of temperature for the Mg 38.84% at. In alloy under the same conditions as those shown in Figure 6.

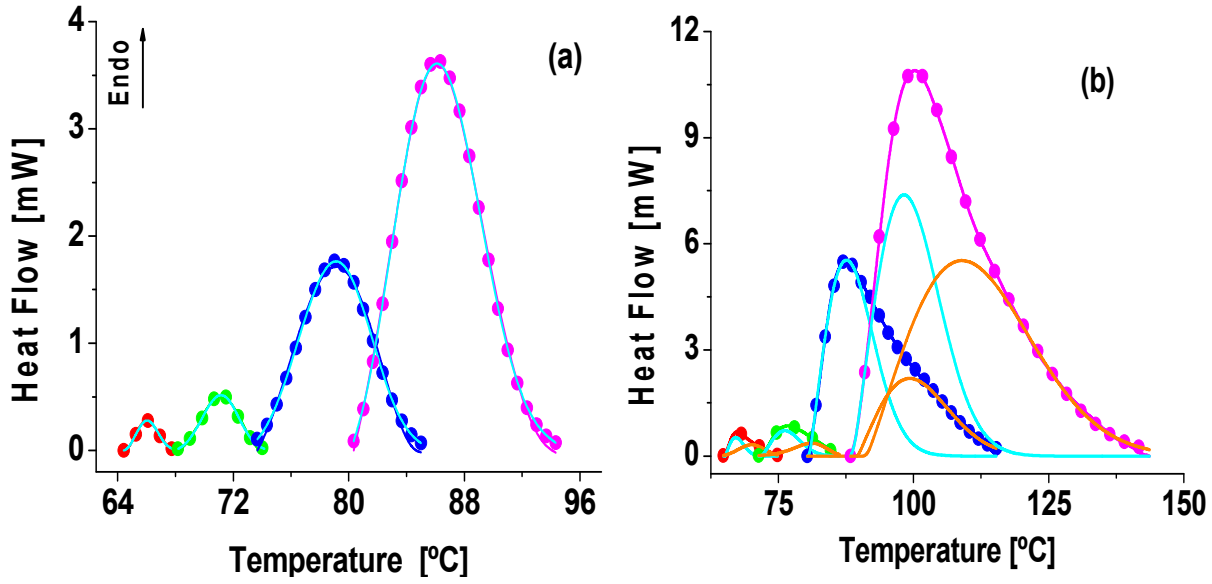

Figure 9. Heat Flow vs. Temperature for a Mg 38.64% at. In alloy using different heat rates. ●: 5ºC min-1, ●: 10ºC min-1, ●: 20ºC min-1, ●: 40ºC min-1. —: First reaction. —: Second reaction. a) Annealing at 300ºC. b) Annealing at 400 ºC.

The results shown in Figure 9 resemble both the behavior and aspect of those of Figure 8; to wit, a single reaction for annealing at 300 °C and a double reaction for annealing at 400 °C. There were, however, particular differences in intensity and peak locations for each heating rate. For this alloy, annealing at 300 °C promoted the formation of phase β2, while quenching and subsequent heating prompted its dissolution, as depicted in Figure 7.a, by means of a single reaction. Annealing at 400 °C, however, promoted the formation of the disordered β phase. Quenching and subsequent heating yielded an asymmetric curve at the beginning, which by deconvolution, generated two reactions: the first one, in agreement with the dissolution of phase β2; and the second, possibly associated with the atomic rearrangement accompanying that phase's ordering process as it moved from the disarray of phase β to the region of coexistence of the ordered β" and β2 phases.

3.3.3 Kinetic parameters

The evaluation of the kinetic parameters was performed in accordance with the previous work of Luiggi et al. [19-21]. First, we estimated the apparent activation energy using Luiggi's Equation (1) [24]:

$$\ln\left(\frac{T^N}{\phi}\right) = C + \frac{Q}{RT} \quad (1)$$

This relationship agrees with the Kissinger Equation [23] when T = Tmax and N = 2. The pairs (Tmax, ϕ) are taken directly from Figures 8 and 9. Figure 10 shows the Kissinger graphs for both alloys.

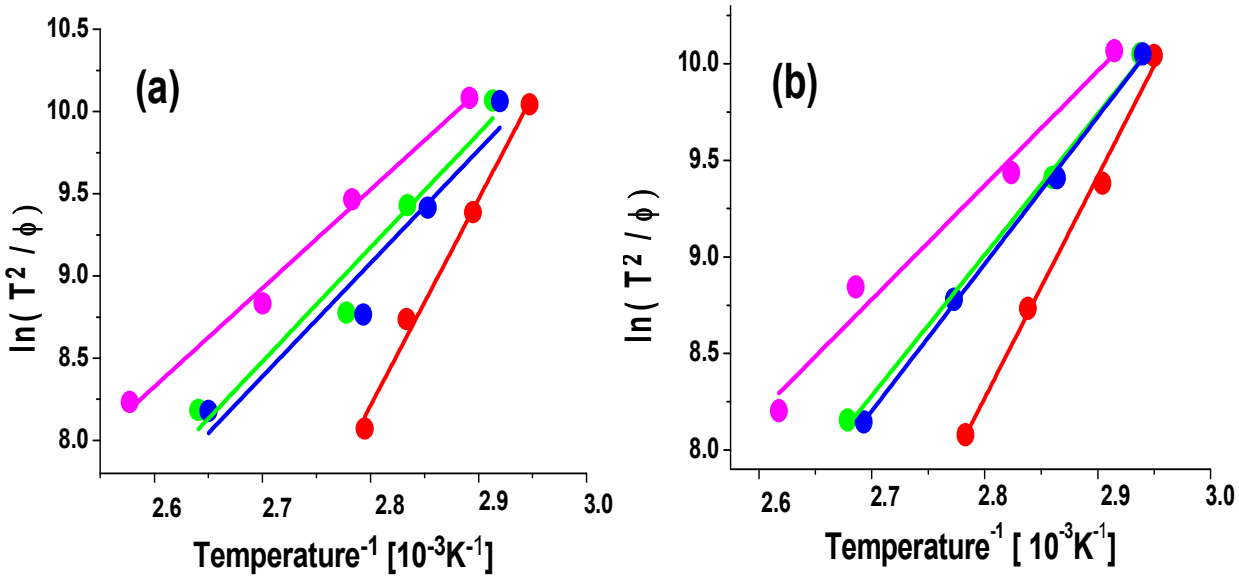

Figure 10. Kissinger plots showing the linear fitting of the pairs (ϕ, Tmax) as a function of the temperature inverse. a. Mg 17.47% at. In b. Mg 38.64% at. In. —: Samples annealed at 300 ºC. —: Samples annealed at 400°C (As Original); —: Samples annealed at 400 ºC (First reaction); —: Samples annealed at 400 ºC (Second reaction).

The linearity shown in these figures points to a thermally activated process, diffusive in character, that associates each reaction with each straight line. The departure from linearity in every case results in an error on the slope of said lines. Table 8 shows the activation energy values obtained from this figure. In the case of annealing at 400 ºC, the result generated using the original thermogram, without deconvolution, is also shown. The reader will be keen to notice that the value of the reported activation energy Q is framed between the Q values obtained from the deconvolved reactions.

To finalize this kinetic study, and in agreement with ITAC guidelines [24] regarding its validity, we evaluated the kinetic triplet by following the methodology described by Luiggi et al. [21, 22].

Well acquainted with the values of Q and using the truncated Sestak-Berggren kinetic function [20,21], we proceeded to fit the experimental or deconvolved data to the following relation:

$$ln\left[\frac{\Delta H\,\Phi}{A(1-\alpha)^n\,\alpha^m}\right] = ln\,A_0 - \frac{Q}{RT} \qquad (2)$$

where ΔH represents the heat flow; A, the area under the heat flow curve; A0, the Arrhenius pre-exponential factor; α, the conversion extension or transformed fraction; and n and m, the Sesták-Berggren parameters.

Maintaining the value of Q within the range of error established in Table 8, the values of both n and m were made to vary until Equation (2) became linear. Any pair (n, m) generating a Q value in that range would be considered valid. Table 9 shows the results obtained after applying linear regression. The table shows the value of the activation energy reproduced in the regression, QSB, as well as Sesták-Berggren coefficients n and m, the Arrhenius prefactor A0, and the correlation coefficient R^2.

Table 8. Activation Energy (Q) deduced from Fig. 9.

Alloy	*Annealing Temperature /ºC*	*Reaction/ Phase*	*Q /kJ*
Mg 17.47 % at. In	300	One phase / β1	104.51 ± 6.56
		As Original	57.62 ± 8.56
	400	First / β1	57.20 ± 9.98
		Second	49.80 ± 2.85
Mg 38.64 % at. In	300	One phase /β2	95.37 ± 4.82
		As Original	59.38 ± 2.04
	400	First / β2	49.14 ± 4.56
		Second / β''	63.36 ± 1.63

Table 9. Kinetic parameters deduced from the combination of the isoconversion method and the Sestak-Berggren model for the different reactions. In column 3 (Alloy / Temper / Reaction (A, T, R)) : First refers to alloy (1: Mg 17.47% In; 2: Mg 38.64% In); Second refers to annealing (1: at 300ºC; 2: at 400 ° C); and Third refers to reaction (0: Non-deconvolved original; 1: First reaction; 2: Second reaction)

Q_{SB} /kJmol^{-1}	Φ / ºCmin^{-1}	*Alloy/ Temper/ Reaction*	*n*	*M*	*Q / kJmol^{-1}*	*A0(min^{-1})*	R^2
105.2637	5		0.725	0.555	104.51 ± 6.6	4.3312E15	0.9590
107.4772	10	111	0.790	0.535		1.6315E15	0.9790
100.2196	20		0.725	0.460		1.2382E13	0.9979
99.6768	40		0.960	0.480		2.8023E12	0.9986
60.3852	5	120	0.730	0.225	57.62 ± 8.56	7.1323E7	0.9078
60.3698	10		1.175	0.030		5.0061E6	0.9913
60.1410	20		1.145	0.000		1.4380E6	0.9798
60.4270	40		1.135	0.120		3.5825E5	0.9642
59.6293	5	121	0.880	0.500	57.20 ± 9.98	1.6330E8	0.9978
55.2731	10		1.010	0.835		3.8504E6	0.9998
54.6664	20		1.050	0.350		8.5318E5	0.9996
55.4943	40		0.995	0.430		2.2417E5	0.9997
48.8935	5	1	0.880	0.575	49.80 ± 2.85	1.8784E6	0.9999
49.2413	10	2	1.525	0.385		1.6695E5	0.9999
50.4438	20	2	1.020	0.320		5.5159E4	0.9962
50.3947	40		0.985	0.360		1.3221E4	0.9964
99.9024	5	2	0.800	0.625	95.37 ± 4.82	7.6008E14	0.9984
98.9168	10	1	0.795	0.655		9.4535E13	0.9992
93.9479	20	1	0.835	0.480		1.9232E12	0.9990
93.0224	40		0.910	0.525		3.2313E11	0.9993
60.2035	5		0.800	0.250	59.38 ± 2.04	1.1359E8	0.8314
60.4051	10	2	0.750	0.325		2.3224E6	0.9206
60.4532	20	2	1.005	0.065		2.2271E6	0.9501
60.4457	40	0	1.220	0.135		5.0049E5	0.9755
49.2040	5		0.875	0.515	49.14 ± 4.56	5.8682E6	0.9874
51.4221	10	2	1.650	0.505		2.5559E6	0.9993
49.5936	20	2	0.955	0.460		1.7877E5	0.9998
47.0636	40	1	0.970	0.460		1.8740E4	0.9997
64.4588	5	2	0.760	0.605	63.36 ± 1.63	6.0034E8	0.9978
63.2744	10	2	0.695	0.705		4.7007E6	0.9989
64.4521	20	2	0.915	0.335		7.9011E6	0.9888
62.2726	40		1.135	0.275		6.9686E5	0.9973

The scant information in the literature regarding the kinetic parameters of this alloy further complicates the interpretation of the results obtained.

In Mg-In alloys whose heat of mixing is negative, the formation of phases occurs by interdiffusion of their components, thus establishing a competition between the phases in formation [14]. This effect is enhanced by milling, which destabilizes the intermetallics present and leads to the formation of extensive solid solutions or amorphous phases [27]. In particular, this fact has generated much ambiguity about the identification of phases, mainly in indium-loaded alloys.

We know, however, that the activation energy for the diffusion of In in Mg is 118.83 kJ/mol in the temperature range between 472 ºC and 610 ºC [28, 29]. The activation energy for the self-diffusion of Mg, between 467-635 ºC, varies between 134.72 and 135.98 $kJmol^{-1}$ [30], while the self-diffusion energy of In between 44 and 144 ºC, is Q = $78.24kJmol^{-1}$. Under this premise we can conclude that the first and only transformation, detected for both alloys annealed at 300 ºC, occurred predominantly by diffusion of In in the Mg matrix; not so for either alloy annealed at 400 ºC, where both the first and second transformation detected occurred by a combination of mechanisms, possibly by the migration of atoms of indium in Mg, and by the self-diffusion of indium in the rich regions of In as detected in the initial micrographs.

This table also highlights:

1. The values of activation energy QSB obtained by fitting are always within the range of error obtained by isoconversion.

2. The pair (n, m) that defines the kinetic function for the same alloy, the same annealing, and the same reaction tended to have similar values within an error range for the different ϕ values considered. Some exceptions in the Alloy / Temper / Reaction column (A, R, T) were observed in: (1, 2, 0) at 5 ºC min^{-1}, (1,2,2) at 10 ºC min^{-1}, (2, 2, 1) at 10 ºC min^{-1}, as were dispersed values in (2, 2, 2). However, since n is an exponent of a growing function, and m an exponent of a decreasing one, both n and m generally tended to be preserved for the same (A, R, T) values and within the respective margin of error.

3. The values of A0 for the reactions following annealing at 300 ºC were much higher than those reported for the reactions generated after annealing at 400 ºC.

4. Finally, the goodness of fit of the calculation, regulated by the value of R^2, indicates fairly accurate results. The greatest deviation from this good behavior (R^2 = 0.8314) was obtained for the alloy Mg 38.84% annealed at 400 ºC and calculated from the non-deconvolved or original data. It is worth noting that overall, all calculations performed on original data are less accurate than those performed on deconvolved data.

3.4 Study of electrical resistivity

Electrical resistivity measurements were performed, as in the case of calorimetry gauging, on compacted samples subjected to 1 hour of annealing at 400 ºC and 300 ºC. The measurements were made from 25 ºC up to the annealing temperature with an increase of 25 ºC, after an isochronous 5-min treatment at each intermediate temperature followed by tempering at 3 ºC in chilled water.

Considering that:

- The diffusion of indium in the magnesium matrix was relatively low (D ~ 10-24 cm^2s^{-1} at 20 ºC [31,32]);

- Microstructural changes occurred mainly during the time that the samples remained at the intermediate annealing temperature, with a low incidence of isochronous cycles on microstructural changes; and

- Also, that at 25 °C (temperature measurement) the lattice effects remained similar after each isochronous step;

We then proceeded to minimize certain common effects by considering the variation of electrical resistivity at each temperature relative to the resistivity value obtained after the initial annealing: $\Delta\rho = (\rho\ (T) - \rho\ (25\ ºC))$. Thus, the main effect reflected in the resistivity measurements would correspond to the microstructural changes.

Figure 11 shows the results for both alloys after the samples were subjected to a sintering treatment of 1 hour at 300 °C. The resistivity variation shows a decrease with a minimum between 200 ºC and 300 ºC accompanied by a rise in resistivity towards the initial value measured. The negative values shown in this figure only indicate that the resistivity at that temperature is lower than the reference resistivity.

For the interpretation of this behavior, we must take into account that the specific resistivity of indium in the magnesium matrix is much higher when the indium atoms are in solid solution than when they are forming precipitates. Hence, the decrease in resistivity indicates the incorporation of indium atoms at a given phase depending on the composition of the alloy, whereas the growth is associated with the dissolution of precipitates, the dissolved atoms passing to the solid solution.

Under this perspective, the decrease in resistivity for both alloys is associated, in the case of the Mg 17.47% at. In alloy, to the development of the β1 phase initiated during the annealing at 300 ºC, which reached its maximum level towards 250 ºC before subsequently starting the dissolution process at higher temperatures. Something similar occurred with the Mg 38.64% at. In alloy, where the annealing at 300 ºC enhanced the formation of phase β2, which at lower T continued to develop up to 200 ºC to then dissolve and increase the electrical resistivity. In principle for this last alloy, we would expect certain changes in the resistivity product of the disorder-order transition when passing from β" (disordered phase) to β2 (ordered phase). Nevertheless, annealing at 300 ºC, very close to the transition temperature in the phase diagram [8], was seemingly not achieved, which supports the premise that the mechanical synthesis of the Mg 38.64% at. In alloy shows an order-disorder transition temperature above 300 ºC.

Figure 12 shows the variation of electrical resistivity for samples subjected to annealing for 1 hour at 400 °C. The main difference of these curves with the one shown in Figure 11 is that at this annealing temperature, the alloy with the lowest In content was definitely placed in the solid solution α, whereas the most charged alloy was located in the disordered β" phase.

For the Mg 17.47% at. In alloy, the electrical resistivity decreased reaching a minimum at 100 ºC, and then rose with some inflection at 325 ºC. The decrease could be attributed to the formation of phase β1 after quenching, whereas its dissolution began to occur above 100 ºC. As for the alloy with the highest content of In, the behavior shown was completely different. A slight increase associated with the atomic rearrangement occurred due to the transition from the disordered β" structure to the ordered β2. A shallow valley between 50 and 150 ºC suggested the presence of an ordered phase within that temperature range, followed by a large valley that reached its minimum value in the vicinity of 225 °C. A maximum resistivity appeared in the vicinity of 325 °C, very close to the transition temperature β"→ β2, followed by a fall in resistivity associated with the consolidation of the initial disordered phase. The interpretation of this behavior is extremely complicated, and we attribute much of it to the order-disorder transition, generated after the initial annealing and tempering.

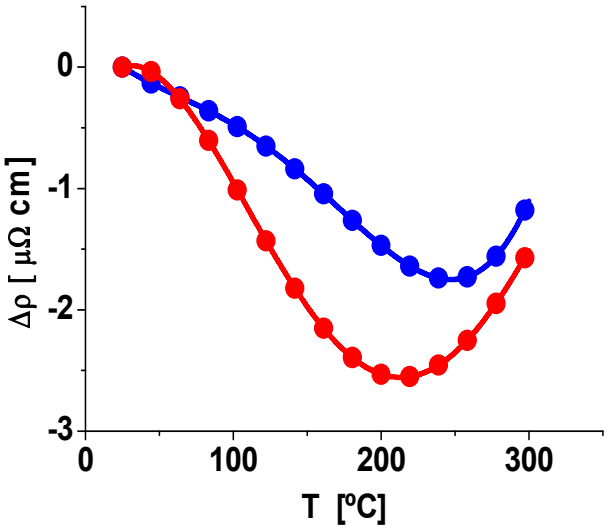

Figure 11. Electrical Resistivity variation versus temperature of samples annealed for 1 hour at 300 ºC, measured at 25 ºC after 5 minutes of isochronal treatment. Mg 17.47% at. In alloy. Mg 38.64% at. In alloy.

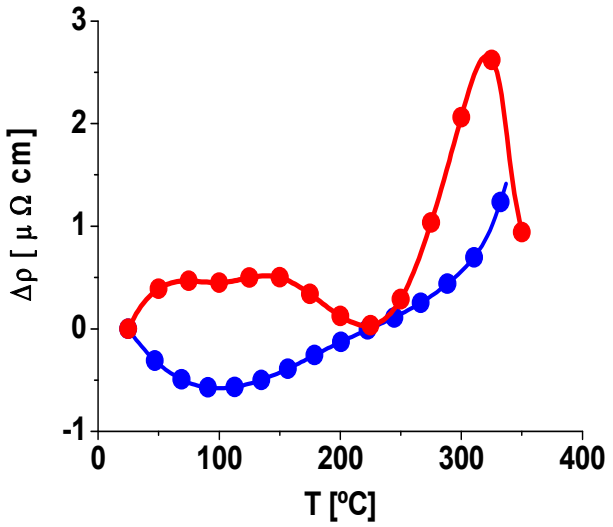

Figure 12. Electrical Resistivity variation versus temperature of samples annealed for 1 hour at 400 ºC, measured at 25 ºC after 5 minutes of isochronal treatment. Mg 17.47% at. In alloy. Mg 38.64% at. In alloy.

4. CONCLUSIONS

Mg 17.74% at. In and mg 38.84% at. In alloys were synthesized by mechanical alloying and studied by optical microscopy, XRD, DSC, and electrical resistivity, the following conclusions having been drawn:

a. After 10 hours of milling, the samples of both alloys were shown to be homogeneous and their granular and sub-granular structures were revealed when treated with a Nital 5% solution.

b. As the synthesis process unfolded, different Mg-In phases were identified by XRD. For the consolidated structure of the Mg 17.47% at. In alloy, the dominant phases were In 0.144 Mg 1.856 and In 0.212 Mg 1.788, which comprised 93.15% of the peak area. The average size of crystallites, not considering lattice strain, evaluated by the Scherrer formula was 41.974 nm, although smaller crystallite sizes were determined for certain planes. A Rietveld analysis showed that both identified phases could well correspond to a single phase since both crystalline structures were hexagonal and their network parameters were within the range of experimental discrepancy. When DICVOL was used, a second orthorhombic phase of undefined nomenclature was also reported. Regarding the Mg 38.84% at. In alloy, the dominant phases were InMg (58.2%), $InMg_3$ (15.8%), and In 0.144 Mg 1.856 (6.5%), achieving an 80.5% matching by Rietveld refinement [17a]. The average size of crystallites evaluated by means of the Scherrer formula [15] was 33.6014 nm, though for certain planes it was possible to determine crystallite sizes of 25.21 nm. Indexing with DICVOL confirmed both the existence of the MgIn phase and the appearance of a new unidentified orthorhombic phase with a much higher atomic volume.

c. The calorimetry measurements showed, for each study condition, a series of endothermic transformations whose temperature ranges are framed within the limits established in the phase diagram of the Mg-In system.

d. The kinetic study of the phases formed at lower temperatures reflected different kinetics from those when the samples were annealed at 300 ºC or 400 ºC. Our results show activation energies in accordance with the diffusion of In in Mg when the samples were previously annealed at 300 ºC; not so for both alloys annealed at 400 ºC, where both the first and second reactions detected occurred by a combination of mechanisms, possibly by the migration of In atoms in Mg and by their self-diffusion in the rich regions of In as detected in the initial micrographs.

e. Resistivity measurements also revealed the effect of annealing, with the resistivity behavior for both alloys being similar when the samples were annealed at 300 °C, suggestive of a bi-phase region at this temperature: (α + β1) for Mg17.47% at. In and (β " + β2) for Mg38.84% at In. In the latter case, this occurred only when the synthesis of the mechanical alloy displaced the solubility limit of β2 in β" at temperatures slightly higher than the established temperature. Contrarily, in samples annealed at 400 ºC, the effect of the order-disorder transition induced a resistivity behavior in the Mg 38.84% at. In alloy different from that shown for the Mg17.47% at. In alloy, where the solid solution α of Mg decomposed itself to make way for phase β1.

5. ACKNOWLEDGMENTS

The authors wish to acknowledge the support of the Universidad de Oriente through POA Project PN 5.5/2010 and the assistance of translator Carlos Mota for reviewing the manuscript.

6. REFERENCES

[1]. Becerra A, Pekguleryuz M. J. Mater. Res. 2008; 23(12): 3379-3386.

[2]. Becerra A, Pekguleryuz M. J. Mater. Res. 2009; 24(5): 1722-1729.

[3]. Murgia F, Weldekidan ET, Stievano L, Monconduit L, Berthelot R. Electrochem. Comm. 2015; 60: 56–59.

[4]. Feschotte P. J. Less-common Metals. 1976; 46: 51–54.

[5]. Hiraga K, Koiwa M, Hirabayashi M. J. Less-Common Metals. 1968; 15(2): 109-119.

[6]. Hume-Rothery W, Raynor GV. The Apparent Sizes of Atoms in Metallic Crystals with Special Reference to Aluminium and Indium, and the Electronic State of Magnesium. Proc. R. Soc. Lond. A. 1940; 177(968): 27-37.

[7]. Kogachi M. J. Phys. Chem. Solids.; 1973; 34(1): 67-75.

[8]. Nayeb-Hashemi AA, Clark JB. Bulletin of alloys phase diagrams. 1985; 6: 149-160.

[9]. Predel B. Phase Equilibria, Crystallographic and Thermodynamic Data of Binary Alloys, Editor. O. Madelung. Landolt-Börnstein, New Series IV/5a, 1991.

[10]. Watanabe Y. Acta. Met. 1975; 23(6): 691-696.

[11]. Curtarolo S, Kolmorov AN, Cocks FH. Calphad. 2005; 29(2): 155-161.

[12]. Pickwick KM, Alexander WA, Gamble RH. Can. J. Chem. 1969; 47(18): 3417-3427.

[13]. Schubert K, Gauzzi F, Frank K. K., Z. Metallkd. 1963; 54: 422-429.

[14]. Liang G, Schulz R. Journal of Metastable and Nanocrystalline Materials. 2002; 12: 93-110.

[15]. Scherrer, P. Bestimmung der Grosse und der Inneren Struktur von Kolloidteilchen Mittels Rontgenstrahlen, Nachrichten von der Gesellschaft der Wissenschaften, Gottingen. Mathematisch-Physikalische Klasse. 1918; 2: 98-100.

[16]. Monshi A, Foroughi MR, Monshi MR. World Journal of Nano Science and Engineering. 2012; 2: 154-160.

[17]. Danilchenko SN, Kukharenko OG, Moseke C, Protsenko IY, Sukhodub LF, Sulkio-Cleff B. Crystal Research and Technology. 2002; 37(11): 1234-1240.

[18]. Rietveld HM. Journal of Applied Crystallography. 1969; 2: 65–71.

[19]. Luiggi NJ. Met. Mater. Trans. B. 2015; 46(3): 1376–1399.

[20]. Luiggi NJ, Valera M. Rev. LatinAm. Metal. Mat. 2017; 37(2): 160-178.

[21]. Luiggi NJ, Valera M. J. Therm. Anal. Calorim. 2017; 130: 1885–1902.

[22]. Sesták J, Berggren G. Thermochim. Acta. 1971; 3(1): 1–12.

[23]. Sesták J. Science of Heat and Thermo physical Studies: a generalized approach to thermal analysis. Elsevier, Amsterdam. 2005.

[24]. Luiggi Met. Mater. Trans. A. 2003; 34A: 2679-2681.

[25]. Kissinger HE. J. Res. Nat. Bur. Stand. 1956; 57: 217–21.

[26]. Vyazovkin S, Burnham AK, Criado JM, Pérez-Maqueda LA, Popescu C, Sbirrazzuoli N. ICTAC Kinetics Committee recommendations for performing kinetic computations on thermal analysis data. Thermochim Acta. 2011; 520 (1-2): 1–19.

[27]. Oehring M, Yan ZH, Klassen T, Bormann R. Phys. Status Solidi A. 1992; 131(2): 671-689.

[28]. Combronde J, Brebec G., Acta Metall. 1972; 20(1): 37–44.

[29]. Lal K., Commis. Energ. At. Report. CEA-R 3136, 1967.

[30]. Shewmon PG. Trans. Met. Soc. AIME.; 1956; 206: 918

[31]. Amonenko M, Blinkin A, Ivantsov IG. Fiz. Metal. Metalloved. 17 (1964) 56-62. Phys. Metals Metallog. 1964; 17:54-59.

[32]. Bi-Cheng Z, Shun-Li S, Yi W, Data Brief. 2015; 5: 900–912.